SIMB Society for Industrial Microbiology and Biotechnology

Journal of Industrial Microbiology and Biotechnology, 2021, 48, kuab029

DOI: 10.1093/jimb/kuab029
Advance access publication date: 18 May 2021
Natural Products – Original Paper

Structure and biosynthesis of sorangipyranone — a new γ-dihydropyrone from the myxobacterial strain MSr12020

Dorothy A. Okoth[1,3,†], Joachim J. Hug[1,3,†], Attila Mándi[4], Tibor Kurtán[4], Ronald Garcia[1,3], Rolf Müller[1,3]

[1]Department Microbial Natural Products, Helmholtz Institute for Pharmaceutical Research Saarland (HIPS), Helmholtz Centre for Infection Research (HZI), Saarland University, Campus E8 1, 66123 Saarbrücken, 66123 Saarbrücken, Germany
[2]Department of Pharmacy, Saarland University, 66123 Saarbrücken, Germany
[3]German Center for Infection Research (DZIF), Partner Site Hannover-Braunschweig Inhoffenstraße 7, 38124 Braunschweig, Germany
[4]Department of Organic Chemistry, University of Debrecen, P. O. Box 400, 4002 Debrecen, Hungary
Correspondence should be addressed to: Department Microbial Natural Products, Helmholtz Institute for Pharmaceutical Research Saarland (HIPS), Helmholtz Centre for Infection Research (HZI), 66123 Saarbrücken, Germany. Phone: +49 681 98896 3000. Email: rolf.mueller@helmholtz-hips.de
[†]These authors contributed equally to this work.

Abstract: Sorangipyranone was isolated as a novel natural product featuring a unique 2,3-dihydro-γ-4*H*-pyrone scaffold from cultures of the myxobacterial strain MSr12020. We report here the full structure elucidation of sorangipyranone by spectroscopic techniques including 2D NMR and high-resolution mass spectrometry together with the analysis of the biosynthetic pathway. Determination of the absolute configuration was performed by time-dependent density functional theory–electronic circular dichroism calculations and determination of the applicability of the Snatzke's helicity rule, to correlate the high-wavelength n→π^* electronic circular dichroism (ECD) transition and the absolute configuration of the 2,3-dihydro-4*H*-γ-pyrone, was done by the analysis of low-energy conformers and the Kohn-Sham orbitals. Sorangipyranone outlines a new class of a γ-dihydropyrone-containing natural product comprised of malonyl-CoA-derived building blocks and features a unique polyketide scaffold. *In silico* analysis of the genome sequence of the myxobacterial strain MSr12020 complemented with feeding experiments employing stable isotope-labeled precursors allowed the identification and annotation of a candidate biosynthetic gene cluster that encodes a modular polyketide synthase assembly line. A model for the biosynthetic pathway leading to the formation of the γ-dihydropyrone scaffold is presented in this study.

Keywords: Myxobacteria, Natural products, γ-Dihydropyrone

Introduction

Natural products are a prolific reservoir of chemical scaffolds featuring unique mode of actions to support the development of new therapeutic options for the treatment of numerous diseases (Huang & Lin, 2017; Newman & Cragg, 2020). Certain groups of underexplored microorganisms located in extreme high salt environments and unconventional habitats such as entomopathogenic bacteria, human commensals, plant and animal endosymbionts are now increasingly investigated as potential source of novel natural products (Garcia et al., 2018; Tobias et al., 2018; Wang et al., 2019; Zhang et al., 2015). Nevertheless, independently growing microorganisms remain among the domain of bacteria the most prolific producers of natural products such as *Streptomyces* sp. and *Bacillus* sp., but also less exploited species like rare actinomycetes, cyanobacteria, and in particular myxobacteria (Demay et al., 2019; Grubbs et al., 2017; Herrmann et al., 2017; Landwehr et al., 2016).

Myxobacteria are not only remarkable Gram-negative soil bacteria featuring unique biological characteristics such as complex chemical communication systems, multicellular development stages and the capability to move in coordinated manner to prey on other microorganisms (Munoz-Dorado et al., 2016), although some recent discoveries did not follow the conventional fruiting body development (Garcia & Müller, 2018). They are considered as one of the most abundant sources for structurally unique natural products with intriguing bioactivities (Herrmann et al., 2017). Hundreds of bioactive secondary metabolites were already isolated and characterized from the order of Myxococcales, albeit the number of investigated myxobacterial strains is rather low in comparison to *Streptomyces* sp. and *Bacillus* sp. (Mohr, 2018). Many myxobacterial natural products feature diverse biological functions through unprecedented mode of actions such as the antiviral aetheramides (Plaza et al., 2012), the immunomodulatory argyrins (Sasse et al., 2002), the cytotoxic pretubulysin (Braig et al., 2014), the antiplasmodial chlorotonil (Gerth et al., 2008), the antifungal nannocystin A (Hoffmann et al., 2015), the antibacterial myxopyronins (Irschik et al., 1983), and the antiwolbachial corallopyronins (Schäberle et al., 2014). Besides the wide range of biological activities, many myxobacterial natural products display elaborate structural features, which often account for their biological function. Multimodular enzyme complexes such as the modular nonribosomal peptide synthetases (NRPSs), polyketide synthases (PKSs) and in particular, PKS–NRPS hybrid systems generate many intriguing secondary metabolites from myxobacteria. These multimodular assembly lines synthesize many different cyclic chemical entities such as thiazole, oxazole, and pyrone heterocycles. A number of α-pyrone containing natural products such as corallopyronins (Jansen et al., 1985), myxopyronins (Irschik et al., 1983; Kohl et al., 1984), phenylnannolones (Ohlendorf et al., 2008), and hyapyrones (Okanya et al., 2014)

Received: December 14, 2020. **Accepted:** May 13, 2021.

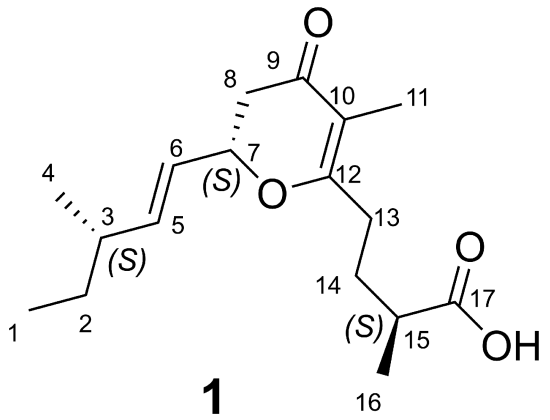

Fig. 1. Chemical structure and carbon numbering of sorangipyranone (**1**).

have been isolated from myxobacteria. Interestingly, the alkenyl α-pyrones like myxopyronins and corallopyronins are cyclized by a ketosynthase (KS) through a head-to-head condensation of two acyl moieties (Pogorevc et al., 2019; Sahner et al., 2015; Sucipto et al., 2013, 2015, 2017). In addition, α-dihydropyrone containing secondary metabolites like the pyrronazols (Jansen et al., 2014; Witte et al., 2017) and ratjadon (Gerth et al., 1995) have been described from myxobacteria.

In contrast to α-pyrones, γ-pyrones are less frequently isolated from myxobacteria with phenoxan (Kunze et al., 1992) being the only known member. Most of these γ-pyrones have been isolated from marine organisms where they act as allomones and defense measures against other microorganisms (Wilk et al., 2009). Examples of natural products that feature a γ-pyrone scaffold include colletotrichins (Gohbara et al., 1978), candelalides (Singh et al., 2001), kalkipyrones (Graber & Gerwick, 1998), verticipyrones (Ui et al., 2006), smenopyrone (Esposito et al., 2018), among others (Wilk et al., 2009). Even less abundant is the γ-dihydropyrone scaffold in natural products where only smenopyrone (which feature a γ-dihydropyrone and a γ-pyrone scaffold) (Esposito et al., 2018), tridachiahydropyrone (Gavagnin et al., 1996), membrenones (Ciavatta et al., 1993), and maurenones (Crossman & Perkins, 2006) have been reported. The discovery of new bioactive natural products featuring a γ-dihydropyrone structure and the elucidation of their biosynthesis are thus valuable findings for medicinal chemistry.

In this study, we describe the discovery and full structure elucidation of sorangipyranone (**1**), from the myxobacterial strain MSr12020 (Fig. 1). An exemplary retrobiosynthetic strategy involving *in silico* genomic investigation and metabolomic feeding analysis of the producer strain MSr12020, revealed the biosynthesis of the γ-dihydropyrone scaffold presented in **1**.

Materials and Methods

Applied Software, DNA Sequence Analysis, and Bioinformatic Methods

The genome of the terrestrial myxobacterial strain MSr12020 (producer strain of **1**), *Polyangium fumosum* DSM 14668 (GenBank: SSMQ01000001.1) and *Polyangium* sp. SDU3 1 (GenBank: SSMR01000017.1) were screened for the presence of BGCs using the antibiotics and secondary metabolite analysis shell (antiSMASH) 5.0 online tool (Blin et al., 2019) and the software Geneious Prime® (Biomatters Ltd., Auckland, New Zealand, 2020.0.5) (Kearse et al., 2012) was used for further biosynthetic investigation such as the biosynthetic gene cluster (BGC) comparison in Supplementary Information Section 2.4. The nucleotide or amino acid sequence of interest was aligned with the basic local alignment search tool (BLAST) against our in-house genome database or the publicly available nucleotide database, in order to find homologous genes or proteins. The functional prediction of open reading frames was performed by using protein blast and/or blastx programs and Pfam (Finn et al., 2016). The nucleotide sequence of the sorangipyranone BGC originating from the myxobacterial strain MSr12020 has been deposited in GenBank under the accession number MW115850.

Maintenance of Bacterial Cultures and Feeding Experiments with Stable Isotope-Labeled Building Blocks

The myxobacterial strain MSr12020 was recognized for its swarming and fruiting body formation in the standard *Escherichia coli* bacterial baiting method (Garcia & Müller, 2014). Repeated transfer of the swarm edge onto fresh-buffered VY/2 agar led to the isolation of this myxobacterium. Based on 16S rRNA gene sequence, the strain MSr12020 belongs to a novel branch in a *Polyangiaceae* family and shows closest neighbor with *Polyangium*.

The myxobacterial strain MSr12020 was routinely cultivated at 30°C in buffered VY/2 (bufVY/2) liquid medium or agar plates [(% = w/v), 0.5% Baker's yeast, 0.05% $CaCl_2$ – $2H_2O$, for agar plate cultures 15 g/l agar (BD) was added, pH adjusted to 7.0 with 10 N KOH before autoclaving]. Liquid cultures were grown in Erlenmeyer flasks on an orbital shaker at 180 rpm for 3–6 days. Genomic DNA of the myxobacterial strain MSr12020 was isolated according a previously established protocol for myxobacteria (Panter et al., 2019) and subjected to whole genome sequencing with Illumina paired-end technology on a MiSeq instrument at the Helmholtz Centre of Infection Research (Braunschweig, Germany). Raw data consisting of 0.96 Gbp reads were assembled using the de novo, parallel, paired-end sequence assembler software ABySS-pe 1.3.4 yielding 62 contigs (Simpson et al., 2009). Since none of these contigs contained a candidate BGC that could be associated with the production of **1**, another sequencing round was performed at Era7 Bioinformatics (Granada, Spain) using long-read technology provided by Pacific Biosciences (PacBio) sequencing (Pacific Biosciences, Menlo Park, CA, USA). Resulting raw reads of 0.79 Gbp and mean read length of 3.7 kbp were assembled with the Canu 1.9 software (Koren et al., 2017) to yield 71 contigs, one of which contained the complete candidate sorangipyranone BGC.

Feeding experiments were performed by cultivating the strain in 20 ml bufVY/2 broth using 300 µl inoculum. The cultures were supplemented with 1 ml (v/v) sterile amberlite resin XAD-16 (Sigma-Aldrich Chemie GmbH, Taufkirchen, Germany) and fed for five consecutive days with 20 µl of a 4 M solution of either malonic acid 2–^{13}C), sodium acetate ($^{13}C_2$) or methionine d_3 at 30°C, at 180 rpm. The combined cells and resin were harvested by centrifugation after 7 days of incubation before extraction. The supernatant was discarded, whereas the combined cells and resin were extracted with a mixture of 25 ml methanol (MeOH) and 25 ml acetone, stirred for 2 hr and filtered through filter paper, and the solvent of the extracts was removed under vacuum. The re-dissolved extracts (2 ml MeOH) were diluted with MeOH (1:3 (extract/MeOH, v/v) and centrifuged, and the supernatant was subjected to high-performance liquid chromatography–mass spectrometry (HPLC–MS) analysis as described further below.

Analysis of Secondary Metabolism of Broth Extracts

The secondary metabolism of broth extracts were analyzed by high-performance liquid chromatography–high-resolution electrospray ionization–diode array-detector–mass spectrometry (HPLC–HRESI–DAD–MS) on a maXis 4G mass spectrometer (Bruker Daltonics, Billerica, MA, USA) coupled with a Dionex UltiMate 3000 Rapid Separation (RS)LC system (Thermo Fisher Scientific, Waltham, MA, USA) using a BEH C18 column (100 × 2.1 mm, 1.7 µm) (Waters, Eschborn, Germany) with a gradient of 5–95% acetonitrile (ACN) + 0.1% formic acid (FA) in H_2O + 0.1% FA at 0.6 ml/min and 45°C over 18 min with ultraviolet (UV) detection by a DAD at 200–600 nm. Mass spectra were acquired from 150 to 2000 *m/z* at 2 Hz. Detection was performed in the positive MS mode. The plugin for Chromeleon Xpress (Thermo Fisher Scientific, Waltham, MA, USA, version 6.8) was used for operation of the Dionex UltiMate 3000 RSLC system. HyStar (Bruker Daltonics, Billerica, MA, USA, version 3.2) was used to operate on the maXis 4G mass spectrometer system. HPLC–MS mass spectra were analyzed with DataAnalysis (Bruker Daltonics, Billerica, MA, USA, version 4.2).

Isolation of Sorangipyranone

The myxobacterial strain MSr12020 was cultivated in 26 l bufVY/2 medium containing 5% (v/v) cell inoculum and 2% (v/v) amberlite resin XAD-16 for 14 d at 160 rpm, 30°C. At the end of fermentation, wet cell mass and adsorbent resin XAD-16 were harvested together by centrifugation at 8000 rpm, 30 min, 4°C. The crude extract was obtained from the fermentation broth by acetone elution, and the extract evaporated under vacuum (10.4 g). The extract was then partitioned between MeOH and *n*-hexane solvents. The MeOH layer was dried under vacuum to yield 6.6 g of extract. This extract was again partitioned in water and chloroform ($CHCl_3$). The $CHCl_3$ layer yielded 2.86 g of extract after the organic solvent was evaporated. The $CHCl_3$ extract was subjected to flash chromatography on an Isolera™One (Biotage, Uppsala, Sweden) with a SNAP 100 g column packed with silica gel (60 Å, 70–230 mesh, 63–200 μm), using *n*-hexane (0.1% FA) as solvent **A**, ethyl acetate (EA) (0.1% FA) as solvent **B**, and MeOH (0.1% FA) as solvent **C**. The flow rate was 50 ml/min, UV/VIS absorption was set at 280 and 350 nm. Collected fractions (45 ml) were monitored on a Dionex UltiMate 3000 RSLC system (Thermo Fisher Scientific, Waltham, MA, USA) coupled to an amaZon ion trap MS (Bruker Daltonics, Billerica, MA, USA). The elution gradient consisted of an initial isocratic mixture of 95:5 (*n*-hexane:EA) for 5 column volumes (CVs), then ramped to 5:95 (*n*-hexane:EA) for 20 CV. This was followed by another isocratic solvent system 100% (EA) for 5 CVs. A final gradient of 5:95 (EA:MeOH) was reached after 5 CVs. Fractions 123–145 was confirmed to contain the compound of interest using high-resolution mass spectrometry. The compound was purified on UltiMate 3000 semi-preparative system coupled to a Thermo Scientific Dionex UltiMate 3000 Series automated fraction collector (Bruker Daltonics, Billerica, MA, USA) using a XSelect CSH C_{18} Prep column, 5 μm, 10 × 250 mm (Waters TM) and eluted with water (0.1% FA) and ACN (0.1% FA). The fractions were monitored by mass spectrometry and by using the UV/VIS detector set at 220, 280, 320, and 400 nm. The gradient program was adjusted to an initial isocratic gradient H_2O:ACN (30:70) for 5 min followed by gradient ramp to 20:80 (H_2O:ACN) in 5 min. The gradient was then maintained to 20:80 (H_2O:ACN) for 18 min and then raised again to 5:95% (H_2O:ACN) in 5 min and held for 2 min before lowering the gradient back to 95:5 (H_2O:ACN) in 1 min. The column was re-equilibrated for 5 min using 95:5 (H_2O:ACN). **1** was detected using mass spectrometry on the Agilent 1100 series (Agilent Technologies, Santa Clara, CA, USA) coupled to the HCT 3D ion trap (Bruker Daltonics, Billerica, MA, USA) or with a UV detector on the Dionex UltiMate 3000 RSLC system by UV absorption at 220, 260, 320, and 400 nm. The HPLC fractions were dried under N_2 resulting in 5.12 mg of compound **1** from fraction four at the retention time of 22.3 min.

NMR-Based Structure Elucidation

The chemical structure of **1** was determined via multidimensional nuclear magnetic resonance (NMR) analysis. ^{1}H-NMR, ^{13}C-NMR, and 2D spectra were recorded at 500 MHz (1H)/175 MHz (^{13}C), conducting an Ascend 500 spectrometer using a cryogenically cooled triple resonance probe (Bruker Biospin, Rheinstetten, Germany). Samples were dissolved in $CDCl_3$. Chemical shifts are reported in ppm relative to tetramethylsilane; the solvent was used as the internal standard (Supplementary Information Section 3.2).

Chiroptical Measurements and Computational Methods

Specific optical rotation measurements of **1** in $CHCl_3$ ($[\alpha]^{25}_D$) were obtained on a Model 341 polarimeter (PerkinElmer Inc., Waltham, MA, USA) in a 100 × 2 mm cell at 25°C. Circular dichroism measurements were performed for **1** at 1 mM in MeOH (190–600 nm) with the J-1500 CD spectrophotometer (JASCO, Easton, MD, USA).

Mixed torsional/low-mode conformational searches were carried out by means of the Macromodel 10.8.011 software using the Merck Molecular Force Field (MMFF) with an implicit solvent model for H_2O applying a 21 kJ/mol energy window (MacroModel, 2015). Geometry re-optimizations of the resultant conformers [AM1 and ωB97X/TZVP with PCM solvent model for MeOH] and time-dependent density functional theory (TDDFT) calculations were performed with Gaussian 09 (Frisch et al., 2013) using various functionals (B3LYP, BH&HLYP, CAM-B3LYP, and PBE0), the TZVP basis set, and the same solvent model as applied in the preceding DFT re-optimization step. Electronic circular dichroism (ECD) spectra were generated as the sum of Gaussians with 3000 cm^{-1} halfheight width, using dipole-velocity-computed rotational strengths (Stephens & Harada, 2010). Boltzmann distributions were estimated from the ωB97X energies. The MOLEKEL and the GaussView software packages were used for visualization of the results (Dennington et al., 2009; Varetto, 2012).

Bioactivity Profiling

For evaluation of antibacterial and antifungal activities of compound **1** *E. coli* DSM 1116^T, *E. coli* JW0451–2 (*acrB*-efflux pump deletion mutant of *E. coli* BW25113), *Pseudomonas aeruginosa* PA14, *Bacillus subtilis* DSM10^T, *Mycobacterium smegmatis* DSM 43756, *Staphylococcus aureus* Newman, *Candida albicans* DSM 1665, *Citrobacter freundii* DSM 30039^T, *Wickerhamomyces anomalus* DSM 6766, and *Acinetobacter baumannii* DSM 30007^T strains were assayed using the microbroth dilution assay as described previously (Okoth D. et al., 2020).

Cytotoxic activity of compound **1** was determined using HCT-116 (human colon carcinoma cell line, DSMZ No. ACC 581) and KB-3-1 (cervix carcinoma cell line, DSMZ No. ACC 158) cells seeded at 6 × 10^3 cells per well of 96-well plates in 180 μl complete medium and treated with compound **1** in serial dilution after 2 hr equilibration. After 5 days of incubation, 20 μl of 5 mg/ml MTT (thiazolyl blue tetrazolium bromide) in phosphate-buffered saline (PBS) was added per well and it was further incubated for 2 hr at 37°C. The

Table 1. Predicted Functions of the Encoded Proteins by the Sorangipyranone Biosynthetic Gene Cluster

Gene	Size (aa)	Proposed function (domains)	Closest homologue	Coverage/identity (%)
orf1	251	Hypothetical protein	WP_136925206.1	63/64.88
orf2	317	HEAT repeat domain-containing protein	WP_136925207.1	70/63.99
orf3	586	PQQ-like beta-propeller repeat protein	WP_136925208.1	92/84.40
orf4	127	Hypothetical protein	WP_136925209.1	99/77.95
orf5	720	Diguanylate cyclase	WP_136925210.1	99/96.39
orf6	387	HAMP domain-containing protein	WP_136925211.1	99/87.60
orf7	241	Transglutaminase family protein	WP_136925212.1	99/92.53
orf8	273	Polysaccharide deacetylase family protein	WP_136925213.1	91/87.70
orf9	193	Hypothetical protein	WP_136925214.1	85/73.65
orf10	488	MBOAT family protein	WP_136925215.1	100/89.37
orf11	99	Hypothetical protein	WP_136925216.1	91/70.65
orf12	126	Hypothetical protein	WP_136925217.1	99/81.89
orf13	209	Hypothetical protein	WP_136925218.1	100/72.25
orf14	365	Tryptophan 2,3-dioxygenase	WP_136925219.1	100/95.07
orf15	545	DUF393 domain-containing protein	WP_136925220.1	98/81.85
orf16	126	DUF393 domain-containing protein	WP_136925220.1	100/86.05
orf17	666	HTTM domain-containing protein	WP_136925238.1	94/89.05
orf18	410	Cytochrome P450 enzyme	WP_136925229.1	95/42.56
orf19	119	Hypothetical protein	WP_136925228.1	81/36.08
orf20	336	Hypothetical protein	WP_146209706.1	95/43.87
spa1	2717	(ACP-KS-AT-AT-DH-ER-KR-ACP)	WP_136925221.1	100/82.18
spa2	1875	(KS-AT-DH-KR-ACP)	WP_136925222.1	99/57.07
spa3	3363	(KS-AT-KR-ACP-KS-AT-DH-KR-ACP)	WP_136925223.1	99/62.92
spa4	3722	(KS-AT-KR-ACP-KS-AT-DH-ER-KR-ACP)	WP_153821597.1	98/60.03
spa5	1962	(KS-AT[a]-DH[a]-KR[a]-ACP-TE)	WP_136925226.1	99/56.95
orf21	140	Hypothetical protein	WP_136925227.1	96/58.09
orf22	379	S8 family serine peptidase	WP_136925537.1	99/97.89
orf23	537	Hypothetical protein	WP_136925539.1	92/69.26
orf24	404	aminotransferase	WP_136925540.1	99/88.59
orf25	628	S8 family serine peptidase	WP_136925541.1	100/86.98
orf26	437	PDZ-containing protein	WP_136925543.1	100/74.94
orf27	898	DNA polymerase I	WP_136925544.1	100/93.88
orf28	91	30S ribosomal protein S20	WP_136925545.1	72/91.04
orf29	490	Hypothetical protein	WP_136925547.1	99/78.67
orf30	195	σ^{70}-family RNA polymerase sigma factor	WP_136925548.1	99/98.97
orf31	431	S41 family peptidase	WP_136925549.1	99/90.02
orf32	411	FAD-binding protein	WP_136925550.1	93/82.64
orf33	532	Glycerol-3-phosphate dehydrogenase/oxidase	WP_136925551.1	99/91.73
orf34	142	MAPEG family protein	WP_136925556.1	99/90.85
orf35	247	Glycosyltransferase family 2 protein	WP_136925557.1	94/96.58

[a]Inactive domains.

medium was discarded, and cells were washed with 100 μl PBS before adding 100 μl isopropanol/10 N HCl (250:1) in order to dissolve formazan granules. The absorbance at 570 nm was measured using the microplate reader Infinite® M200Pro (Tecan Group Ltd., Männedorf, Switzerland), and cell viability was expressed as a percentage relative to the respective MeOH control. IC_{50} values were determined by sigmoidal curve fitting.

Results and Discussion

Isolation and Structural Elucidation of Sorangipyranone

The high-resolution mass spectrum of the compound indicated a molecular formula $[M + H]^+$ of $C_{17}H_{27}O_4$ consistent with a molecular mass of 295.1904 Da identified with the retention time of 10.33 min from the crude extract of the producer strain MSr12020. In addition two ions *m/z* 589.3735 of molecular formula $C_{34}H_{53}O_8$ and 277.1799 of molecular formula $C_{17}H_{25}O_3$ corresponding to the $[2M + H]^+$ and $[M\text{-}H_2O + H]^+$ ions were observed. The UV/VIS absorption at 338 nm due to the $n\rightarrow\pi^*$ transition (R-band) and 282 nm due to $\pi\rightarrow\pi^*$ transition (K-band) indicated the presence of an α,β-unsaturated ketone moiety (Brewster, 2002) (Fig. S18). The ^{1}H NMR was characterized by two olefinic protons in an *E* configuration (δ_H 5.52 (dd, J = 6.5, 15.5 Hz) and δ_H 5.62 (dd, J = 7.5, 15.5 Hz), an oxygenated methine δ_H 4.67 (m, H-7), three methylenes δ_H 2.50 (2H, m, H-8), δ_H 2.38 (2H, m, H-13), (δ_H 1.30 (2H, m, H-2), and inequivalent methylene protons δ_H 1.93 (1H, m, H-14) and 1.68 (1H, m, H-14), two methine protons δ_H 2.04 (1H, q, H-3) and δ_H 2.48 (1H, m, H-15), and four methyl groups δ_H 1.70 (3H, s, H-11), 1.22 (3H, d, J = 7.1 Hz, H-16), 0.98 (3H, d, J = 6.8 Hz, H-4), and 0.83 (3H, t, J = 7.5 Hz, H-1). The ^{13}C NMR showed 17 carbons consisting of three oxygenated quaternary carbons δ_C 192.7 (C-9), 180.5 (C-17), 171.7 (C-12), an sp-hybridized carbon δ_C 110.3 (C-10), olefinic carbons δ_C 141.0 (C-5) and 125.4 (C-6), oxygenated methine carbon δ_C 78.7 (C-7), two methine carbons δ_C 38.7 (C-15) and 38.1 (C-3), four methylenes δ_C 41.5(C-8), 30.0 (C-14), 30.01 (C-15), 29.3 (C-2), and four methyl carbons δ_C 19.7 (C-4), 17.2 (C-16), 11.7 (C-1), 9.2 (C-11). The combination of correlation spectroscopy (COSY), heteronuclear single quantum coherence/correlation (HSQC), and heteronuclear multiple bond correlation (spectroscopy) (HMBC) (Table S5) revealed the

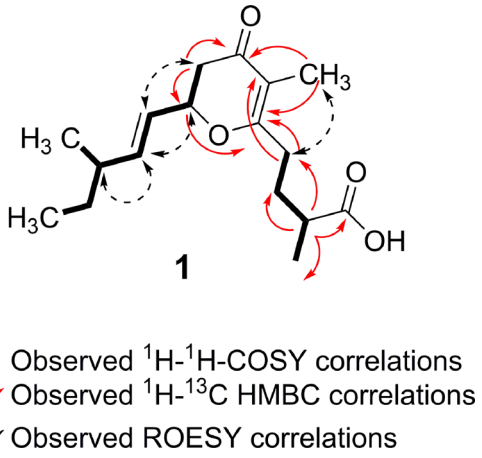

Fig. 2. Key COSY, HMBC, and ROESY correlations for **1**.

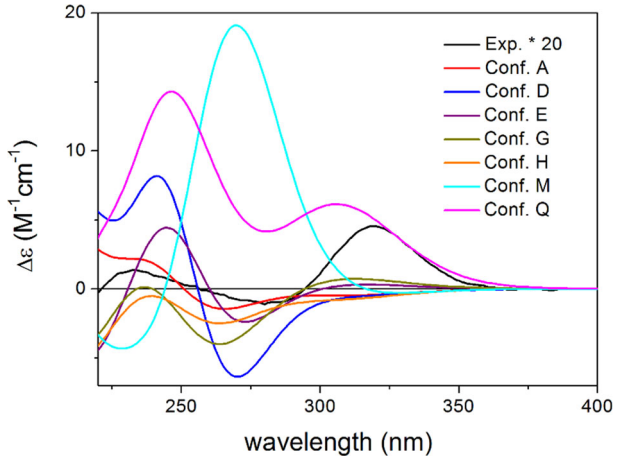

Fig. 3. Experimental ECD spectrum of **1** in MeOH [Exp. *20 (multiplied by 20)] compared with the B3LYP/TZVP PCM/MeOH ECD spectra of several low-energy ωB97X/TZVP PCM/MeOH conformers of (3*S*,7*S*,15*S*)-**1**.

connectivity of the various segments within the chemical structure of **1** (Fig. 2). ^{1}H–^{1}H–COSY correlations observed between H-1/H-2, H-2/H-3, H-3/H-4, H-3/H-5, H-5/H-6, H-6/H-7, and H-7/H-8 enabled the identification of the partial structure –(CH_3-CH_2-CH(CH_3)-CH═CH-CH(O)-CH_2)–. Further ^{1}H-^{1}H-COSY between H-13/H-14, H-14/H-15 and H-15/H-16 confirmed the partial structure –(CH_2-CH_2-CH (CH_3))–. The resonance signals δ_C 192.7 (C-9), 110.3 (C-10), 171.7 (C-12) are consistent with an α,β-unsaturated ketone in γ-dihydropyrones (Ciavatta et al., 1993; Crossman & Perkins, 2006) while the δ_C 180.5 (C-17) was assigned as a carbonyl carbon of carboxylic acid. The HMBC correlations observed between the H-7 and C-8, C-9 and C-12 and H-8 and C-9 and C-10 thereby lead to the assignment of the dihydropyrone ring skeleton. Additional HMBC cross peaks between H-14 methylene, H-15 methine, and H-16 methyl protons with C-17 carboxylic acid permitted the assignment of the position of the carboxylic group. The attachment of the side-chain at C-12 was based on HMBC interactions of H-13 methylene protons with the dihydropyrone carbons C-10 and C-12. The dihydropyrone moiety consisting of the oxygenated methine δ_C 78.7 (C-7), methylene δ_C 41.5 (C-8), and the α,β-unsaturated ketone δ_C 192.7 (C-9), 110.3 (C-10), 171.7 (C-11). The HMBC correlation of the methyl group with the dihydropyrone α,β-unsaturated ketone moiety allowed the positioning of the methyl group. Although Rotating-frame Overhauser effect spectroscopy (ROESY) correlations were observed between the H-7 methine (δ_H 4.67 (m)), and H-5 olefinic proton (δ_H 5.62) and H-5 and H-3 methine proton (δ_H 2.04) (Fig. 2), the observed correlations could not conclusively reveal the relative configuration at the C-3 and C-7. In fact, computational chemistry calculations, ECD, and the study of the biosynthetic pathway of **1** provided further insights concerning the stereochemistry of the chiral centers as outlined below. The configuration of the C-5, C-6 double bond was assigned as *E* based on the large coupling constant ($^{3}J_{H\text{-}5,H\text{-}6}$ = 15.5 Hz). Compound **1** had negative specific rotation with an $[\alpha]^{25}_{D}$ value of –34 ($CHCl_3$, *c* = 1.0).

The ECD spectrum of **1** was recorded in MeOH and it showed a positive Cotton effect (CE) at 318 and 233 nm, and a negative one at 280 nm {ECD λ[nm] (Δε): 318 (+0.23), 280 (–0.06), 233 (+0.07)} (Fig. 3, and Figs. S20 and S23). Compound **1** contains an α,β-unsaturated ketone chromophore as a subunit of the 2,3-dihydro-4*H*-γ-pyrone moiety, which is expected to exert a major effect on the ECD spectrum. Snatzke established a relationship between the chirality of cyclic aryl ketones and their high-wavelength n→π^* CEs (Snatzke, 1965), which was extended to correlate the helicity of the heterocyclic ring and the sign of the n→π^* CE in flavanones (Gaffield, 1970), 3-hydroxyflavanones (Gaffield, 1970), 2-alkylchromanones (McGahren et al., 1972), and isoflavanones (Galeffi et al., 1997; Kurtán et al., 2012; Slade et al., 2005). According to this rule, *P*-helicity of the heterocyclic ring adopting envelope conformation is manifested in a positive n→π^* CE above 300 nm. Although the 2,3-dihydro-4*H*-γ-pyrone chromophore lacks the condensed benzene ring, it might be considered the simplified analogue of the above benzene-condensed heterocycles. Based on the positive CE at 318 nm, the extension of the helicity rule to the 2,3-dihydro-4*H*-γ-pyrone chromophore would suggest *P*-helicity of **1** with (7*S*) absolute configuration equatorial orientation of the C-7 side-chain.

In order to predict the absolute configuration of C-7 and check the possible extension of the chromanone helicity rule to the 2,3-dihydro-4*H*-γ-pyrone chromophore, the solution TDDFT–ECD method (Mándi & Kurtán, 2019; Superchi et al., 2018) was applied on compound **1**. The presence of the carbon-carbon double bond attached to C-7 chirality center and the remote carboxyl group may also interfere with the application of the extended helicity rule (Mándi et al., 2016). The initial MMFF conformational search of (3*S*,7*S*,15*S*)-**1** resulted in 2160 conformer clusters in a 21 kJ/mol energy window. To reduce the number of conformers, a semi-empirical AM1 re-optimization (Kicsák et al., 2018) was applied and the structures were re-clustered by neglecting the orientation of the C-1 carbon (Zhou et al., 2014). Lowest energy representatives of the resultant 642 conformer clusters were re-optimized at the ωB97X/TZVP (Jeng-Da Chai & Martin Head-Gordon, 2008) PCM/MeOH level yielding 18 conformers over 1% Boltzmann population (Fig. S21). ECD spectra were computed at four levels of theory for each structure to check the consistency of the different levels. Based on the similarity of the computed ECD spectra and the geometry of the conformers, three conformer groups (A–C) were identified and there were additional individual conformers (conf. D, E, M, Q), which showed markedly different ECDs from those of the conformer groups (Fig. S22).

The heterocyclic ring adopted *P*-helicity ($\omega_{C\text{-}12,O,C\text{-}7,C\text{-}8} > 0$, +50.1° in conformer A) with equatorial orientation of the C-7 side-chain in 16 conformers (52.2% sum population) out of the 18 computed ones and the two *M*-helicity conformers had very small populations (1.3% and 1.0%). In spite of the *P*-helicity of the heterocyclic ring, the four lowest energy conformers A–D had a negative CE for the characteristic highest wavelength n→π^*

transition. In these conformers, the hydroxyl hydrogen of the carboxyl group was coordinating to the pyrone oxygen forming an eight-membered chelate and probably this was responsible for the negative n→π^* transition. Conformer D differed from conformers A–C in the orientation of the vinyl group in the C-7 side-chain, which is reflected in different shape and relative intensities of the ECD transitions. Conformer E and group B conformers had a positive n→π^* CE and their carboxyl group did not form hydrogen bond with the pyrone oxygen, while group C conformers had negative n→π^* CE, although they did not have intramolecular hydrogen bond. The computed ECD spectra of the individual conformers suggested that the sign of the n→π^* CE was not determined exclusively by the helicity of the heterocyclic ring but the conformation of the C-7 and C-12 side-chains containing a vinyl and a chelating carboxyl group had to be also considered. Although most of the low-energy conformers gave only partial agreement (Fig. 3), the Boltzmann-weighted ECD spectrum reproduced well the experimental spectrum allowing to predict the absolute configuration of **1** as (3*S*,7*S*,15*S*) (Fig. S23).

For the assignment of the three low-energy ECD transitions, the computed Kohn–Sham orbitals of the lowest energy conformer (conf. A) were investigated (Fig. S24). The 318 nm ECD transition was found to be of n→π^* origin (HOMO-1 → LUMO) but besides the nonbonding orbital of the carbonyl oxygen, the ground-state orbital also had a contribution from the vinyl π orbital. The 280 nm transition is a pure $\pi\rightarrow\pi^*$ transition of the α,β-unsaturated ketone chromophore (HOMO → LUMO), and almost all the *P*-helicity conformers reproduced well its negative CE. The 233 nm band derives from a $\pi\rightarrow\pi^*$ transition, in which the ground-state orbital is mostly the vinyl π orbital with small contribution from the oxygen nonboning orbital. In summary, our ECD analysis revealed that the 280 nm ECD transition is not of pure n→π^* origin and the Snatzke's helicity rule cannot be applied, since besides the helicity of the heterocyclic ring, the conformation of the C-7 and C-12 side-chains have also significant effect on the characteristic ECD transition.

In order to corroborate the theoretical assignment of the absolute configuration of **1** (in particular the stereocenters at C-3 and C-15), we further focused on a retrobiosynthetic strategy; first we conducted metabolomic feeding analysis of the producer strain MSr12020 to obtain hints concerning the incorporated building blocks and to hypothesize the underlying biosynthetic origin of **1**. These findings in turn provided the foundation for the subsequent *in silico* genomic investigation and elucidation of the biosynthesis of the γ-dihydropyrone scaffold presented in **1**.

Feeding Experiments and *In Silico* Biosynthetic Investigation of Sorangipyranone

MSr12020 fermentation cultures were supplemented with malonic acid 2-^{13}C and subsequent MS analysis indicated incorporation of the malonate building blocks resulting in +1, +2 and +3 Da mass shifts in the isotopic pattern of **1** (Fig. S1). Stable isotope-labeled sodium acetate ($^{13}C_2$) was incorporated into the γ-dihydropyrone natural product, resulting in significant mass shift in the isotopic pattern of **1,** ranging from +1 up to +10 Da (Fig. S2). Furthermore, MSr12020 fermentation cultures supplemented with methylmalonate d_3 display mass shifts of +3, +6, and +9 Da in the isotopic pattern of **1** (Fig. S3).

All three feeding experiments confirm that **1** most likely originates from a PKS biosynthetic pathway. The methyl groups of **1** arise from methylmalonate building blocks and presumably not from S-adensoyl-L-methionine (SAM)-dependent methyltransferases, which are the most common type of methyltransferases involved in the biosynthesis of natural products (Liscombe et al., 2012). This assumption is supported by the fact, that supplementation with L-methionine (methyl-^{13}C) featured no observable incorporation into the γ-dihydropyrone scaffold (Fig. S4).

The structure of **1** alongside with the conducted feeding experiments indicated that a PKS pathway might account for the biosynthesis of **1**. Isolation and sequencing the genome of the myxobacterial strain MSr12020 revealed according to the antibiotics and secondary metabolite analysis shell (antiSMASH) a candidate PKS gene cluster responsible for the biosynthesis of **1**. This candidate BGC contains according the automated antiSMASH annotation 23 open reading frames (*orf1–18* and *spa1–5*) and comprises 63 693 bp (Table 1 and Fig. 4A).

The investigation of publicly available genome sequences revealed that the myxobacterial strains *P. fumosum* DSM 14668 and *Polyangium* sp. SDU3-1 harbors each a BGC related to the proposed gene cluster of **1.** However, the modular architecture of the candidate BGC in *P. fumosum* DSM 14668 seems to be significantly truncated and might be involved in the biosynthesis of a natural product with a structure distinct from **1**. In contrast, the candidate BGC from *Polyangium* sp. SDU3-1 shares higher similarity with the proposed gene cluster of **1**, since the number of functional modules is identical, but differences in substrate specificity, and the presence or absence of functional accessory domains implies that the generated natural product might be different from **1** (Fig. S9).

The genes *spa1–5* encode one PKS loading module and seven PKS extension modules (Fig. 4B). According to the identified candidate BGC, the biosynthesis of **1** is initiated by loading acetyl-coenzyme A (CoA) onto the acyl carrier protein (ACP) of the loading module, and proceeds with the incorporation of three malonyl-CoA and three methylmalonyl-CoA extender units. The predicted substrate specificities of acyl transferase (AT) domains (Supplementary Information Section 2.1) and the presence of optional ketoreductase (KR), dehydratase (DH), and enoyl reductase (ER) domains support the proposed formation of **1** (Fig. 4B).

During the first elongation step a methylmalonyl-CoA building block is incorporated into the polyketide backbone to yield the biosynthesis intermediate **i**. The AT domain specificity of module 1 encoded by *spa1*, underlines the incorporation of a methylmalonate as extender unit (Supplementary Information Section 2.1). Since module 1 performs a full reductive conversion of the incorporated methylmalonyl-CoA building block catalyzed through the KR, DH, and ER domains, the stereospecificity of the methyl group in intermediate **i** (and **1**) is dictated by the ER domain present in module 1. According to a previous mutagenesis study in a modular PKS system, an unique tyrosine residue in the ER active site determines the chirality of the introduced methyl branch (Kwan et al., 2008). Since this position in the active site of the ER domain in module 1 is occupied by a tyrosine residue, the carbon featuring the methyl branch is most probably *S*-configured (Supplementary Information Section 2.2); in contrast in those ER domains producing a (2*R*)-methyl branch, a valine residue or rarely alanine or phenylalanine is present at this position (Kwan et al., 2008).

The second extension step is catalyzed by the PKS module 2 (encoded by *spa2*), which incorporates a malonyl-CoA extender unit to yield intermediate **ii**. The configurational assignment of the double bond between C-5 and C-6 in compound **1** conducted via NMR measurement is in good agreement with the *in silico* identified biosynthesis.

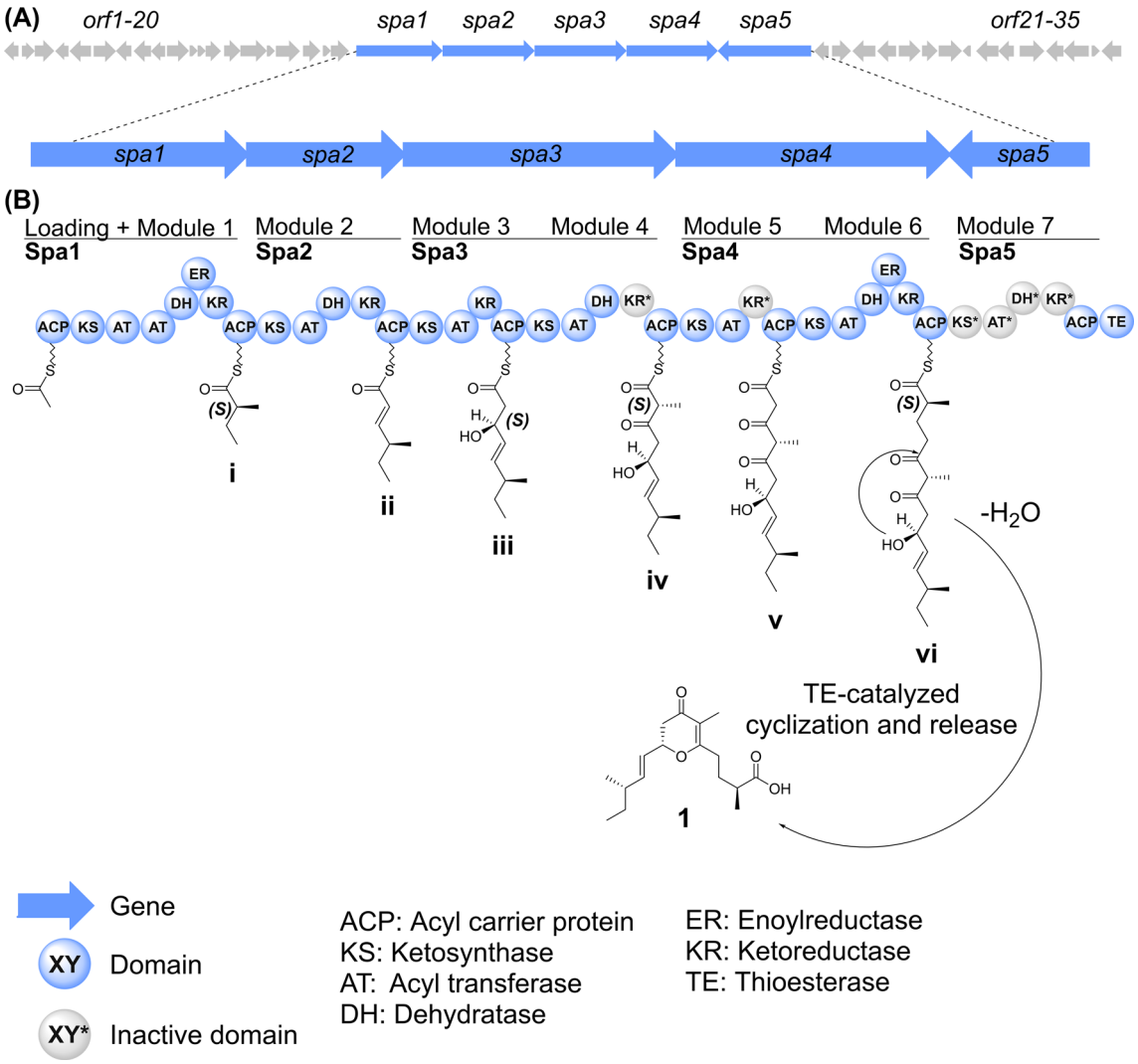

Fig. 4. (A) *In silico* identified biosynthetic gene cluster and (B) the proposed biosynthetic pathway in MSr12020 leading to the formation of **1**.

During the biosynthesis of **1**, the double bond between C-5 and C-6 is determined by the respective KR domain in module 2, which generates a hydroxyl-acyl intermediate to subsequently undergo syn coplanar elimination of the β-hydroxy group and the L-α-proton (Valenzano et al., 2010). Since this DH domain-catalyzed elimination can only bind to its substrate and proceed its catalytic conversion when the substituents of its α- and β-carbons are eclipsed, the absolute configuration of the catalytic product can be predicted a priori. The elimination reaction will yield an *E*-configured double bond from a substrate possessing a D-β-hydroxy group and a *Z*-configured double bond from a substrate possessing an L-β-hydroxy group. Since the KR domain in module 2 was identified as B-type KR, the hydroxyl-acyl intermediate features a D-β-hydroxy group (S-configured), which accounts for the *E*-configuration in intermediate **ii** (and **1**) (Supplementary Information Section 2.3).

Since PKS module 3 harbors only an optional KR domain, the biosynthetic intermediate **iii** would feature a chiral carbon on C-7. The suggested stereochemistry of the secondary hydroxyl group on intermediate **iii**, was assigned as D-configured (S configuration on intermediate **iii**), since the KR domain on module 3 is a B-type KR, which yields the α-substituent in D-orientation (A-type KR yields the α-substituent in L-orientation) (Supplementary Information Section 2.3).

The next extension steps catalyzed by the PKS module 4 and 5 incorporates methylmalonyl-CoA and malonyl-CoA to yield intermediate **iv** and **v**, respectively. It is worth mentioning that the inactive KR domains in module 4 and 5 provide the unreduced C-9 and C-12 ketones, which are necessary for the dihydropyrone ring formation through cyclization and subsequent dehydration (see below). It can be assumed that these two KR domains are inactive because both lack the NADPH-binding motif, and the catalytic tyrosine and serine residue (Supplementary Information Section 2.3). The last elongation step of the polyketide backbone is catalyzed through module 6 encoded by *spa4*, which incorporates another methylmalonyl-CoA building block to yield the linear precursor **vi**. As mentioned above, the ER domain of module 6 determines the absolute configuration of the carbon featuring the methyl branch of intermediate **vi** and **1** (Supplementary Information Section 2.2).

In contrast to the modules 1–6, module 7 is presumably not catalyzing the incorporation of another extension unit and is assumed to be skipped such as described for the biosynthesis of the nonribosomal peptide myxochromide S (Wenzel et al., 2006)

and the polyketide pikromycin (Beck et al., 2002). According to the primary amino acid sequence, the KS domain of module 7 does not feature the catalytic machinery comprised of a cysteine (from a TA**C**SSS motif) as well as two histidines (from EA**H**GTG and KSNIG**H**T motifs) (Keating-Clay, 2012). Therefore, the KS domain is probably not catalytically active. Furthermore, the DH, KR, and AT domains in module 7 are severely truncated and most likely not catalytically functional.

Only the thioesterase (TE) domain in module 7 features sequence motifs required for catalytic action; the GxSxG motif closely located to the *N*-terminus and the GxH motif located nearby the *C*-terminus both harboring the catalytic serine and the histidine, respectively (Keating-Clay, 2012). Therefore, it seems likely, that the TE domain in module 7 catalyzes the cyclization and release of the intermediate **vi** to finally yield **1**.

1 was evaluated for its biological function via numerous bioactivity assays including antifungal assays, cytotoxicity testing against HCT-116 and KB3.1 cell line and antibacterial tests against various Gram-negative and Gram-positive bacterial strains. The natural product **1** inhibited proliferation of HCT-116 and KB3.1 at IC_{50} of 30.0 and 102.5 µg/ml, respectively. The compound was active against *A. baumannii* at a minimal inhibitory concentration (MIC) of 256 µg/ml.

Nevertheless, **1** was not active against *E. coli* DSM 1116^T, *E. coli* JW0451–2, *P. aeruginosa* PA14, *B. subtilis* DSM10^T, *M. smegmatis* DSM 43756^T, *S. aureus* Newman, *C. albicans* DSM 1665, *C. freundii* DSM 30039^T, *W. anomalus* DSM 6766 and *A. baumannii* DSM 30007^T (MIC > 256 µg/ml).

Natural products with α-pyrone scaffolds originating from myxobacteria or γ-dihydropyrone-containing natural products originating from different microorganisms exhibited antifungal and antibacterial activities as outlined above (Jansen et al., 1985, 2014; Kunze et al., 1992). However, given the rather low activity in the assays performed, the biological function of this new compound family with its first member **1** is likely to have a distinctive biological function that is currently unknown.

Conclusions

In summary, this study describes the isolation, full structure elucidation and revealed the biosynthesis of the new natural product **1** from the myxobacterial strain MSr12020. We reported here to the best of our knowledge for the first time the isolation of a myxobacterial natural product featuring a γ-dihydropyrone scaffold, which is an uncommon finding for natural products. In addition, feeding experiments alongside with *in silico* genome analysis provided not only a plausible biosynthetic route to the γ-dihydropyrone scaffold in **1**, but also allowed to predict the stereochemical configuration of **1**.

These findings provide an excellent basis for further biosynthetic investigations of **1**, and pave the way for future genetic and biotechnological approaches. The identified BGC could be heterologously expressed in the myxobacterial model host *Myxococcus xanthus* DK1622 (Hug & Müller, 2020) to produce γ-dihydropyrone containing compounds for medicinal chemistry. Biotechnological and genetic modification of the BGC and the associated microorganism could be applied to provide different compounds featuring γ-dihydropyrone scaffolds for semisynthetic strategies—this would be an alternative for total synthesis and biology-oriented synthesis approaches (van Hattum & Waldmann, 2014; Wilk et al., 2009). In closing, this study emphasizes the importance of the new myxobacterial strain MSr12020 to gain access to notable natural products featuring interesting chemical scaffolds.

Acknowledgments

The authors thank Stefanie Schmidt, Irene Kochems, and Victoria Schmitt for performing bioactivity assays, Sergi Herve Akone for scientific advice, and Nestor Zaburannyi for bioinformatic support. The Governmental Information-Technology Development Agency (KIFÜ) is acknowledged for CPU time.

Supplementary Material

Supplementary material is available online at *JIMB* (*www.academic.oup.com/jimb*).

Data availability

The dataset generated during the study is available in the GenBank respository under the accession number MW115850. Further data supporting the findings of this study are available from the corresponding author on reasonable request.

Funding

This work was financially supported by the Deutsche Forschungsgemeinschaft (DFG), the Bundesministerium für Bildung und Forschung (BMBF), and the Deutsches Zentrum für Infektionsforschung Standort Hannover-Braunschweig. Tibor Kurtán and Attila Mándi thank the National Research Development and Innovation Office (NKFI K120181 and FK134653) for the financial support. Dorothy A. Okoth acknowledges funding from a Humboldt Foundation postdoctoral fellowship. Joachim J. Hug acknowledges funding from a PhD fellowship of Boehringer Ingelheim Fonds.

Conflict of Interest

The authors declare no conflict of interest.

References

Beck, B. J., Yoon, Y. J., Reynolds, K. A., & Sherman, D. H. (2002). The hidden steps of domain skipping: Macrolactone ring size determination in the pikromycin modular polyketide synthase. *Chemistry & Biology*, 9, 575–583.

Blin, K., Shaw, S., Steinke, K., Villebro, R., Ziemert, N., Lee, S. Y., Medema, M. H., & Weber, T. (2019). Antismash 5.0: Updates to the secondary metabolite genome mining pipeline. *Nucleic Acids Research* 47(W1), W81–W87. https://doi.org/10.1093/nar/gkz310.

Braig, S., Wiedmann, R. M., Liebl, J., Singer, M., Kubisch, R., Schreiner, L., Abhari, B. A., Wagner, E., Kazmaier, U., Fulda, S., & Vollmar, A. M. (2014). Pretubulysin: A new option for the treatment of metastatic cancer. *Cell Death & Disease*, 5, e1001. https://doi.org/10.1038/cddis.2013.510.

Brewster, J. H. (2002). Organic conformational analysis and stereochemistry from circular dichroism spectroscopy. *Journal of the American Chemical Society*, 124(12), 3186–3187. https://doi.org/10.1021/ja015298n [by David A. Lightner (University of Nevada) and Jerome E. Gurst (University of West Florida). Wiley-VCH: New York. 2000. xvi + 488 pp. $94.95. ISBN: 0-471-35405-8].

Ciavatta, M.L., Trivellone, E., Villani, G., & Cimino, G. (1993). Membrenones: New polypropionates from the skin of the mediterranean mollusc *Pleurobranchus membranaceus*. *Tetrahedron Letters*, 34(42), 6791–6794. https://doi.org/10.1016/S0040-4039(00)61703-3.

Crossman, J. S. & Perkins, M. V. (2006). Total synthesis and structural elucidation of (–)-maurenone. *The Journal of Organic Chemistry*, 71(1), 117–124. https://doi.org/10.1021/jo051753c.

Demay, J., Bernard, C., Reinhardt, A., & Marie, B. (2019). Natural products from cyanobacteria: Focus on beneficial activities. *Marine Drugs*, 17(6), 320. https://doi.org/10.3390/md17060320.

Dennington, R., Keith, T., & Millam, J. (2009). *GaussView, Version* 5, Semichem Inc..

Esposito, G., Teta, R., Della Sala, G., Pawlik, J. R., Mangoni, A., & Costantino, V. (2018). Isolation of smenopyrone, a bis-γ-pyrone polypropionate from the caribbean sponge *Smenospongia aurea*. *Marine Drugs*, 16(8), 285. https://doi.org/10.3390/md16080285.

Finn, R. D., Coggill, P., Eberhardt, R. Y., Eddy, S. R., Mistry, J., Mitchell, A. L., Potter, S. C., Punta, M., Qureshi, M., Sangrador-Vegas, A., Salazar, G. A., Tate, J., & Bateman, A. (2016). The Pfam protein families database: Towards a more sustainable future. *Nucleic Acids Research*, 44(D1), D279–D285. https://doi.org/10.1093/nar/gkv1344.

Frisch, M. J., Trucks, G. W., Schlegel, H. B., Scuseria, G. E., Robb, M. A., Cheeseman, J. R., Scalmani, V., Barone, G., Mennucci, B., Petersson, G. A., Nakatsuji, H., Caricato, M., Li, X., Hratchian, H. P., Izmaylov, A. F., Bloino, J., Zheng, G., Sonnenberg, J. L., Hada, M., … Fox, D. J. (2013). *Gaussian 09 (Revision E. 01)*. Gaussian, Inc..

Gaffield, W. (1970). Circular dichroism, optical rotatory dispersion and absolute configuration of flavanones, 3-hydroxyflavanones and their glycosides: Determination of aglycone chirality in flavanone glycosides. *Tetrahedron*, 26(17), 4093–4108. https://doi.org/10.1016/S0040-4020(01)93050-9.

Galeffi, C., Rasoanaivo, P., Federici, E., Palazzino, G., Nicoletti, M., & Rasolondratovo, B. (1997). Two prenylated isoflavanones from *Millettia pervilleana*. *Phytochemistry*, 45(1), 189–192. https://doi.org/10.1016/S0031-9422(96)00773-X.

Garcia, R., La Clair, J. J., & Müller, R. (2018). Future directions of marine myxobacterial natural product discovery inferred from metagenomics. *Marine Drugs*, 16(9), 303. https://doi.org/10.3390/md16090303.

Garcia, R. & Müller, R. (2014). The Family Myxococcaceae. In E. Rosenberg, E. F. DeLong, S. Lory, E. Stackebrandt, & F. Thompson (Eds.), *The Prokaryotes: Deltaproteobacteria and Epsilonproteobacteria* (pp. 191–212). Springer. https://doi.org/10.1007/978-3-642-39044-9_303.

Garcia, R. & Müller, R. (2018). *Simulacricoccus ruber* gen. Nov., sp. Nov., a microaerotolerant, non-fruiting, myxospore-forming soil myxobacterium and emended description of the family *Myxococcaceae*. *International Journal of Systematic and Evolutionary Microbiology*, 68(10), 3101–3110. https://doi.org/10.1099/ijsem.0.002936.

Gavagnin, M., Mollo, E., Cimino, G., & Ortea, J. (1996). A new γ-dihydropyrone-propionate from the caribbean sacoglossan *Tridachia crispata*. *Tetrahedron Letters*, 37(24), 4259–4262. https://doi.org/10.1016/0040-4039(96)00811-8.

Gerth, K., Schummer, D., Hofle, G., Irschik, H., & Reichenbach, H. (1995). Ratjadon: A new antifungal compound from Sorangium cellulosum (myxobacteria) production, physio-chemical and biological properties. *Journal of Antibiotics*, 48(9), 973–976. https://doi.org/10.7164/antibiotics.48.973.

Gerth, K., Steinmetz, H., Höfle, G., & Jansen, R. (2008). Chlorotonil A, a macrolide with a unique gem-dichloro-1,3-dione functionality from *Sorangium cellulosum*, So ce1525. *Angewandte Chemie, International Edition in English*, 47(3), 600–602. https://doi.org/10.1002/anie.200703993.

Gohbara, M., Kosuge, Y., Yamasaki, S., Kimura, Y., Suzuki, A., & Tamura, S. (1978). Isolation, structures and biological activities of colletotrichins, phytotoxic substances from *Colletotrichum nicotianae*. *Agricultural and Biological Chemistry*, 42(5), 1037–1043. https://doi.org/10.1271/bbb1961.42.1037.

Graber, M. A. & Gerwick, W. H. (1998). Kalkipyrone, a toxic γ-pyrone from an assemblage of the marine cyanobacteria *Lyngbya majuscula* and *Tolypothrix* sp. *Journal of Natural Products*, 61(5), 677–680. https://doi.org/10.1021/np970539j.

Grubbs, K. J., Bleich, R. M., Santa Maria, K. C., Allen, S. E., Farag, S., Shank, E. A., & Bowers, A. A. (2017). Large-scale bioinformatics analysis of *Bacillus* genomes uncovers conserved roles of natural products in bacterial physiology. *MSystems*, 2(6), e00040–17. https://doi.org/10.1128/mSystems.00040-17"}https://doi.org/10.1128/mSystems.00040-17.

Herrmann, J., Fayad, A. A., & Müller, R. (2017). Natural products from myxobacteria: Novel metabolites and bioactivities. *Natural Product Reports*, 34(2), 135–160. https://doi.org/10.1039/C6NP00106H.

Hoffmann, H., Kogler, H., Heyse, W., Matter, H., Caspers, M., Schummer, D., Klemke-Jahn, C., Bauer, A., Penarier, G., Debussche, L., & Brönstrup, M. (2015). Discovery, structure elucidation, and biological characterization of nannocystin A, a macrocyclic myxobacterial metabolite with potent antiproliferative properties. *Angewandte Chemie, International Edition in English*. 54(35), 10145–10148. Advance online publication. https://doi.org/10.1002/anie.201411377.

Huang, T. & Lin, S. (2017). Microbial natural products: A promising source for drug discovery. *Applied Microbiology and Biotechnology*, 1(2), 5. https://doi.org/10.21767/2576-1412.100005.

Hug, J. J. & Müller, R. (2020). Host development for heterologous expression and biosynthetic studies of myxobacterial natural products: 6.09. In H.-W. (B.) Liu & T. P. Begley (Eds.), *Comprehensive natural products III* (Vol. 6, pp. 149–216). Elsevier. https://doi.org/10.1016/B978-0-12-409547-2.14818-8.

Irschik, H., Gerth, K., Höfle, G., Kohl, W., & Reichenbach, H. (1983). The myxopyronins, new inhibitors of bacterial RNA synthesis from *Myxococcus fulvus* (Myxobacterales). *The Journal of Antibiotics (Tokyo)*, 36(12), 1651–1658. https://doi.org/10.7164/antibiotics.36.1651.

Jansen, R., Höfle, G., Irschik, H., & Reichenbach, H. (1985). Antibiotika aus Gleitenden Bakterien, XXIV. Corallopyronin A, B und C – drei neue Antibiotika aus *Corallococcus coralloides* Cc c127 (Myxobacterales). *Liebigs Annalen Der Chemie*, 1985(4), 822–836. https://doi.org/10.1002/jlac.198519850418.

Jansen, R., Sood, S., Huch, V., Kunze, B., Stadler, M., & Müller, R. (2014). Pyrronazols, metabolites from the myxobacteria *Nannocystis pusilla* and *N. exedens* are unusual chlorinated pyrone-oxazole-pyrroles. *Journal of Natural Products*, 77(2), 320–326. https://doi.org/10.1021/np400877r.

Jeng-Da, Chai & Martin, Head-Gordon (2008). Systematic optimization of long-range corrected hybrid density functionals. *The Journal of Chemical Physics*, 128(8), 84106. https://doi.org/10.1063/1.2834918.

Kearse, M., Moir, R., Wilson, A., Stones-Havas, S., Cheung, M., Sturrock, S., Buxton, S., Cooper, A., Markowitz, S., Duran, C., Thierer, T., Ashton, B., Meintjes, P., & Drummond, A. (2012). Geneious basic: An integrated and extendable desktop software platform for the organization and analysis of sequence data. *Bioinformatics*, 28(12), 1647–1649. https://doi.org/10.1093/bioinformatics/bts199.

Keating-Clay, A. T. (2012). The structures of type I polyketide synthases. *Natural Product Reports*, 29(10), 1050–1073. https://doi.org/10.1039/c2np20019h.

Kicsák, M., Mándi, A., Varga, S., Herczeg, M., Batta, G., Bényei, A., Borbás, A., & Herczegh, P. (2018). Tricyclanos: Conformationally constrained nucleoside analogues with a new heterotricycle obtained from a D-ribofuranose unit. *Organic & Biomolecular Chemistry*, 16(3), 393–401. https://doi.org/10.1039/c7ob02296d.

Kohl, W., Irschik, H., Reichenbach, H., & Höfle, G. (1984). Antibiotics from gliding bacteria. XXll. The biosynthesis of myxopyronin A, an antibiotic from *Myxococcus fulvus* strain Mx f50. *Liebigs Annalen Der Chemie*, 1984(6), 1088–1093.

Koren, S., Walenz, B. P., Berlin, K., Miller, J. R., Bergman, N. H., & Phillippy, A. M. (2017). Canu: Scalable and accurate long-read assembly via adaptive k-mer weighting and repeat separation. *Genome Research*, 27(5), 722–736. https://doi.org/10.1101/gr.215087.116.

Kunze, B., Jansen, R., Pridzun, L., Jurkiewicz, E., Hunsmann, G., Hofle, G., & Reichenbach, H. (1992). Phenoxan, a new oxazole-pyrone from myxobacteria: Production, antimicrobial activity and its inhibition of the electron transport in complex I of the respiratory chain. *Journal of Antibiotics*, 45(9), 1549–1552.

Kurtán, T., Antus, S., & Pescitelli, G. B. (2012). *Comprehensive chiroptical spectroscopy: Applications in stereochemical analysis of synthetic compounds, natural products, and biomolecules* (Vol. 2, pp. 73–114). John Wiley & Sons, Inc.

Kwan, D. H., Sun, Y., Schulz, F., Hong, H., Popovic, B., Sim-Stark, J. C., Haydock, S. F., & Leadlay, P. F. (2008). Prediction and manipulation of the stereochemistry of enoylreduction in modular polyketide synthases. *Chemistry & Biology*, 15(11), 1231–1240. https://doi.org/10.1016/j.chembiol.2008.09.012.

Landwehr, W., Wolf, C., & Wink, J. (2016). Actinobacteria and myxobacteria—Two of the most important bacterial resources for novel antibiotics. *Current Topics in Microbiology and Immunology*, 398, 273–302. https://doi.org/10.1007/82_2016_503.

Liscombe, D. K., Louie, G. V., & Noel, J. P. (2012). Architectures, mechanisms and molecular evolution of natural product methyltransferases. *Natural Product Reports*, 29(10), 1238–1250. https://doi.org/10.1039/c2np20029e.

MacroModel (2015). Schro¨dinger, LLC, 2015, http://www.schrodinger.com/MacroModel. Accessed 8 April 2021.

Mándi, A. & Kurtán, T. (2019). Applications of OR/ECD/VCD to the structure elucidation of natural products. *Natural Product Reports*, 36(6), 889–918. https://doi.org/10.1039/c9np00002j.

Mándi, A., Swamy, M. M. M., Taniguchi, T., Anetai, M., & Monde, K. (2016). Reducing molecular flexibility by cyclization for elucidation of absolute configuration by CD calculations: Daurichromenic acid. *Chirality*, 28(6), 453–459. https://doi.org/10.1002/chir.22606.

McGahren, W. J., Ellestad, G. A., Morton, G. O., & Kunstmann, M. P. (1972). LL-D253α, -β, and -γ, novel chromanones from the fungus *Phoma pigmentivora*. *The Journal of Organic Chemistry*, 37(10), 1636–1639. https://doi.org/10.1021/jo00975a039.

Mohr, K. I. (2018). Diversity of myxobacteria—We only see the tip of the Iceberg. *Microorganisms*, 6(3), 84. https://doi.org/10.3390/microorganisms6030084.

Munoz-Dorado, J., Marcos-Torres, F. J., Garcia-Bravo, E., Moraleda-Munoz, A., & Perez, J. (2016). Myxobacteria: Moving, killing, feeding, and surviving together. *Frontiers in Microbiology*, 7, 781. https://doi.org/10.3389/fmicb.2016.00781.

Newman, D. J. & Cragg, G. M. (2020). Natural products as sources of new drugs over the nearly four decades from 01/1981 to 09/2019. *Journal of Natural Products*, 83(3), 770–803. https://doi.org/10.1021/acs.jnatprod.9b01285.

Ohlendorf, B., Leyers, S., Krick, A., Kehraus, S., Wiese, M., & König, G. M. (2008). Phenylnannolones A–C: Biosynthesis of new secondary metabolites from the myxobacterium *Nannocystis exedens*. *Chembiochem*, 9(18), 2997–3003. https://doi.org/10.1002/cbic.200800434.

Okanya, P. W., Mohr, K. I., Gerth, K., Kessler, W., Jansen, R., Stadler, M., & Müller, R. (2014). Hyafurones, hyapyrrolines, and hyapyrones: Polyketides from *Hyalangium minutum*. *Journal of Natural Products*, 77(6), 1420–1429. https://doi.org/10.1021/np500145f.

Okoth, D. A., Hug, J. J., Garcia, R., Spröer, C., Overmann, J., & Müller, R. (2020). 2-Hydroxysorangiadenosine: Structure and biosynthesis of a myxobacterial sesquiterpene–nucleoside. *Molecules (Basel, Switzerland)*, 25(11), 2676. https://doi.org/10.3390/molecules25112676.

Panter, F., Krug, D., & Müller, R. (2019). Novel methoxymethacrylate natural products uncovered by statistics-based mining of the *Myxococcus fulvus* secondary metabolome. *ACS Chemical Biology*, 14(1), 88–98. https://doi.org/10.1021/acschembio.8b00948.

Plaza, A., Garcia, R., Bifulco, G., Martinez, J. P., Hüttel, S., Sasse, F., Meyerhans, A., Stadler, M., & Müller, R. (2012). Aetheramides A and B, potent HIV-inhibitory depsipeptides from a myxobacterium of the new genus "*Aetherobacter*". *Organic Letters*, 14(11), 2854–2857. https://doi.org/10.1021/ol3011002.

Pogorevc, D., Panter, F., Schillinger, C., Jansen, R., Wenzel, S. C., & Müller, R. (2019). Production optimization and biosynthesis revision of corallopyronin A, a potent anti-filarial antibiotic. *Metabolic Engineering*, 55, 201–211. https://doi.org/10.1016/j.ymben.2019.07.010.

Sahner, J. H., Sucipto, H., Wenzel, S. C., Groh, M., Hartmann, R. W., & Müller, R. (2015). Advanced mutasynthesis studies on the natural α-pyrone antibiotic myxopyronin from *Myxococcus fulvus*. *Chembiochem*, 16(6), 946–953. https://doi.org/10.1002/cbic.201402666.

Sasse, F., Steinmetz, H., Schupp, T., Petersen, F., Memmert, K., Hofmann, H., Heusser, C., Brinkmann, V., Matt, P. von, Höfle, G., & Reichenbach, H. (2002). Argyrins, immunosuppressive cyclic peptides from myxobacteria. I. Production, isolation, physicochemical and biological properties. *Journal of Antibiotics Tokyo*, 55(6), 543–551.

Schäberle, T. F., Schiefer, A., Schmitz, A., König, G. M., Hoerauf, A., & Pfarr, K. (2014). Corallopyronin A—A promising antibiotic for treatment of filariasis. *International Journal of Medical Microbiology*, 304(1), 72–78. https://doi.org/10.1016/j.ijmm.2013.08.010.

Simpson, J. T., Wong, K., Jackman, S. D., Schein, J. E., Jones, S. J. M., & Birol, I. (2009). ABySS: A parallel assembler for short read sequence data. *Genome Research*, 19(6), 1117–1123. https://doi.org/10.1101/gr.089532.108.

Singh, S. B., Zink, D. L., Dombrowski, A. W., Dezeny, G., Bills, G. F., Felix, J. P., Slaughter, R. S., & Goetz, M. A. (2001). Candelalides A–C: Novel diterpenoid pyrones from fermentations of *Sesquicillium candelabrum* as blockers of the voltage-gated potassium channel Kv1.3. *Organic Letters*, 3(2), 247–250. https://doi.org/10.1021/ol006891x.

Slade, D., Ferreira, D., & Marais, J. P. J. (2005). Circular dichroism, a powerful tool for the assessment of absolute configuration of flavonoids. *Phytochemistry*, 66(18), 2177–2215.

Snatzke, G. (1965). Circulardichroismus—X: Modifizierung der octantenregel für α,β-ungesättigte ketone: cisoide enone, dienone und arylketone. *Tetrahedron*, 21(3), 439–448. https://doi.org/10.1016/S0040-4020(01)98284-5.

Stephens, P. J. & Harada, N. (2010). ECD cotton effect approximated by the Gaussian curve and other methods. *Chirality*, 22(2), 229–233. https://doi.org/10.1002/chir.20733.

Sucipto, H., Pogorevc, D., Luxenburger, E., Wenzel, S. C., & Müller, R. (2017). Heterologous production of myxobacterial α-pyrone antibiotics in *Myxococcus xanthus*. *Metabolic Engineering*, 44, 160–170. https://doi.org/10.1016/j.ymben.2017.10.004.

Sucipto, H., Sahner, J. H., Prusov, E., Wenzel, S. C., Hartmann, R., Koehnke, J., & Müller, R. (2015). *In Vitro* reconstitution of α-pyrone ring formation in myxopyronin biosynthesis. *Chemical Science*, 6(8), 5076–5085. https://doi.org/10.1039/C5SC01013F.

Sucipto, H., Wenzel, S. C., & Müller, R. (2013). Exploring chemical diversity of a-pyrone antibiotics: Molecular basis of myxopyronin biosynthesis. *Chembiochem*, 14(13), 1581–1589. https://doi.org/10.1002/cbic.201300289.

Superchi, S., Scafato, P., Gorecki, M., & Pescitelli, G. (2018). Absolute configuration determination by quantum mechanical calculation of chiroptical spectra: Basics and applications to fungal metabolites. *Current Medicinal Chemistry*, 25(2), 287–320.

Tobias, N. J., Shi, Y.-M., & Bode, H. B. (2018). Refining the natural product repertoire in entomopathogenic bacteria. *Trends in Microbiology*, 26(10), 833–840. https://doi.org/10.1016/j.tim.2018.04.007.

Ui, H., Shiomi, K., Suzuki, H., Hatano, H., Morimoto, H., Yamaguchi, Y., Masuma, R., Sunazuka, T., Shimamura, H., Sakamoto, K., Kita, K., Miyoshi, H., Tomoda, H., & Omura, S. (2006). Verticipyrone, a New NADH-fumarate reductase inhibitor, produced by *Verticillium* sp. Fki-1083. *The Journal of Antibiotics*, 59(12), 785–790. https://doi.org/10.1038/ja.2006.103.

Valenzano, C. R., You, Y.-O., Garg, A., Keatinge-Clay, A., Khosla, C., & Cane, D. E. (2010). Stereospecificity of the dehydratase domain of the erythromycin polyketide synthase. *Journal of the American Chemical Society*, 132(42), 14697–14699. https://doi.org/10.1021/ja107344h.

van Hattum, H. & Waldmann, H. (2014). Biology-oriented synthesis: Harnessing the power of evolution. *Journal of the American Chemical Society*, 136(34), 11853–11859. https://doi.org/10.1021/ja505861d.

Varetto, U. (2012). *Molekel 5.4. 0.8*. Swiss National Supercomputing Centre.

Wang, L., Ravichandran, V., Yin, Y., Yin, J., & Zhang, Y. (2019). Natural products from mammalian gut microbiota. *Trends in Biotechnology*, 37(5), 492–504. https://doi.org/10.1016/j.tibtech.2018.10.003.

Wenzel, S. C., Meiser, P., Binz, T. M., Mahmud, T., & Müller, R. (2006). Nonribosomal peptide biosynthesis: Point mutations and module skipping lead to chemical diversity. *Angewandte Chemie, International Edition in English*, 45(14), 2296–2301. https://doi.org/10.1002/anie.200503737.

Wilk, W., Waldmann, H., & Kaiser, M. (2009). Γ-Pyrone natural products—A privileged compound class provided by nature. *Bioorganic and Medicinal Chemistry*, 17(6), 2304–2309. https://doi.org/10.1016/j.bmc.2008.11.001.

Witte, S. N. R., Hug, J. J., Géraldy, M., Müller, R., & Kalesse, M. (2017). Biosynthesis and total synthesis of pyrronazol B: A secondary metabolite from *Nannocystis pusilla*. *Chemistry—A European Journal*, 23(63), 15917–15921. https://doi.org/10.1002/chem.201703782.

Zhang, X., Wei, W., & Tan, R. (2015). Symbionts, a promising source of bioactive natural products. *Science China Chemistry*, 58(7), 1097–1109. https://doi.org/10.1007/s11426-015-5398-6.

Zhou, Z.-F., Kurtán, T., Yang, X.-H., Mándi, A., Geng, M.-Y., Ye, B.-P., Taglialatela-Scafati, O., & Guo, Y.-W. (2014). Penibruguieramine A, a novel pyrrolizidine alkaloid from the endophytic fungus *Penicillium* sp. Gd6 associated with Chinese mangrove *Bruguiera gymnorrhiza*. *Organic Letters*, 16(5), 1390–1393. https://doi.org/10.1021/ol5001523.